www.amlett.com, www.amlett.org, DOI: 10.5185/amlett.2012.9428 Published online by the VBRI press in 2013

Study of strontium doping on the structural and magnetic properties of $YMnO_3$ ceramics

Radheshyam Rai[1*], Indrani Coondoo[1], M. A. Valente[2], Andrei L. Kholkin[1]

[1]*Department of Materials and Ceramics Engineering and CICECO, University of Aveiro, 3810-193 Aveiro, Portugal*
[2]*Departamento de Fisica, I3N, Universidade de Aveiro, Campus Universitario de Santiago, 3810-193 Aveiro, Portugal*

[*]Corresponding author. E-mail: radheshyamrai@ua.pt

Received: 24 September 2012, Revised: 09 October 2012 and Accepted: 17 October 2012

ABSTRACT

Structural and Magnetic properties are investigated for the Sr doped $YMnO_3$ samples with different composition synthesized by a solid state reaction method. Sr doped $YMnO_3$ is the most distorted perovskite of the $RMnO_3$ series (R=rare earths); the observed sinusoidal magnetic structure is in contrast with those exhibited by the less-distorted members, which are commensurate-type antiferromagnetic structures. A typical anti ferromagnetic (AFM) to paramagnetic (PM) phase transition is observed for the sample with concentration x = 0.12 and the Néel temperature (T_N) is about 160 K. With decreasing temperature, the sample with x = 0.12 exhibit a magnetic transition from a paramagnetic (PM) to a ferromagnetic (FM) state. Copyright © 2013 VBRI press.

Keywords: Sr doping; magnetic properties; $YMnO_3$; microstructure.

Radheshyam Rai had joined the National Physical Laboratory in 2003 during the Ph.D. He did his Ph.D. from Magadh University Bodh Gaya in 2004 in physics. During his Ph.D. he worked on PLZT ferroelectric materials with different dopants and also worked on LPG and CNG gas sensor devices in National Physical Laboratory and Indian Institute of Technology, New Delhi. He has quite significant *list of publications and research activities*. After that he joined as Young Scientist in Department of Physics, Indian Institute of Technology, Delhi, India. During this period he worked on ferroelectromagnetic materials for devices application. Presently he is working as Post-doctoral fellow at Universidade de Aveiro, under the Fundacão para a Ciênciaea Tecnologia, Lisboa, Portugal. During this period he is working on nonlead based piezoelectric materials for energy harvesting and ferromagnetic materials.

Introduction

Recently, $YMnO_3$ (YMO) has attracted interest as a multifunctional material for applications owing to the existence of coupling between electrical and magnetic orders [**1**]. Such electromagnetic multiferroics which exhibit simultaneous ferroelectricity and magnetism can be exploited in both electrical and magnetic applications [**2-3**]. Among the single phase multiferroic materials, the un-doped manganites with small size rare-earth cations (like Tb, Dy, Ho and so on) are one of the most fascinating families. Not only the hexagonal $RMnO_3$ (*R* denotes rare-earth cations) [**4–9**], but also the RMn_2O_5 series [**10–13**] show multiferroicity.

The multiferroic YMO belongs to the class of h-$RMnO_3$ compounds having a two-dimensional layered hexagonal structure, with the Mn–Mn distance along the *c*-axis direction (6.07 Å) being much longer than that in the *ab* plane (3.55 Å) [**14-15, 3**]. Electrical polarization in YMO is along the hexagonal c axis [**1**] whereas the magnetic moments of Mn^{3+} lie in the perpendicular plane, forming a triangular, geometrically frustrated network of anti-ferromagnetic coupled spins [**16-17**]. YMO exhibits a high ferroelectric transition temperature (T_C~900 K) and a low antiferromagnetic transition temperature (T_N ~70 K) [**18**]. The studies on $YMnO_3$, $HoMnO_3$ and $LuMnO_3$ indicated that the values of ordering temperatures are associated with the size of R^{3+} ion. In addition, the size effects in yttrium based manganites were also reported [**19-20**]. Much of experimental work on the Ca and Sr doped-YMO ceramics has attracted considerable attention owing to their colossal-magnetoresistance (CMR) effects [**21**]. Study of the CMR effects in doped manganites could benefit our understanding of strongly correlated electron systems. It was believed that the spin structure and electronic properties of $R_{1-x}A_xMnO_3$ (*R*, A denotes rare-earth and divalent ions, respectively) were correlated via the double-exchange mechanism [**21–24**]. However, Millis *et al* argued that double exchange alone could not explain the CMR effects in $R_{1-x}A_xMnO_3$, and proposed that a strong electron–phonon coupling, e.g. via Jahn–Teller effects, should play an important role [**25–27**]. A magnetic and electronic phase diagram was established for $R_{2/3}A_{1/3}MnO_3$ to represent lattice effects [**28-29**]. It was also shown that the tolerance factor was a key parameter in determining the magnetic and

 Copyright © 2013 VBRI press.

transport properties of the compounds, because it affects the bending of Mn–O–Mn bonds and therefore the one electron bandwidth. Archibald et al suggested an unusual trapping out of mobile holes above T_c due to local, static Jahn–Teller deformation [**30**]. Multifunctional magnetic nanoparticles have emerged as one of the important futuristic material for variety of applications starting from data storage, security/sensors to biomedical applications. Magnetic nanoparticles (MNPs) with interesting structure advantages have been developed a number of obvious biomedical applications [31-34]. In this study, we investigated the synthesis of the orthorhombic series of $Y_{1-x}Sr_xMnO_3$ perovskite structure by partial substitution of strontium on $YMnO_3$. The mechanism of multiferroicity in annealed $Y_{1-x}Sr_xMnO_3$ sample was systematically investigated by performing structural and magnetic analyses.

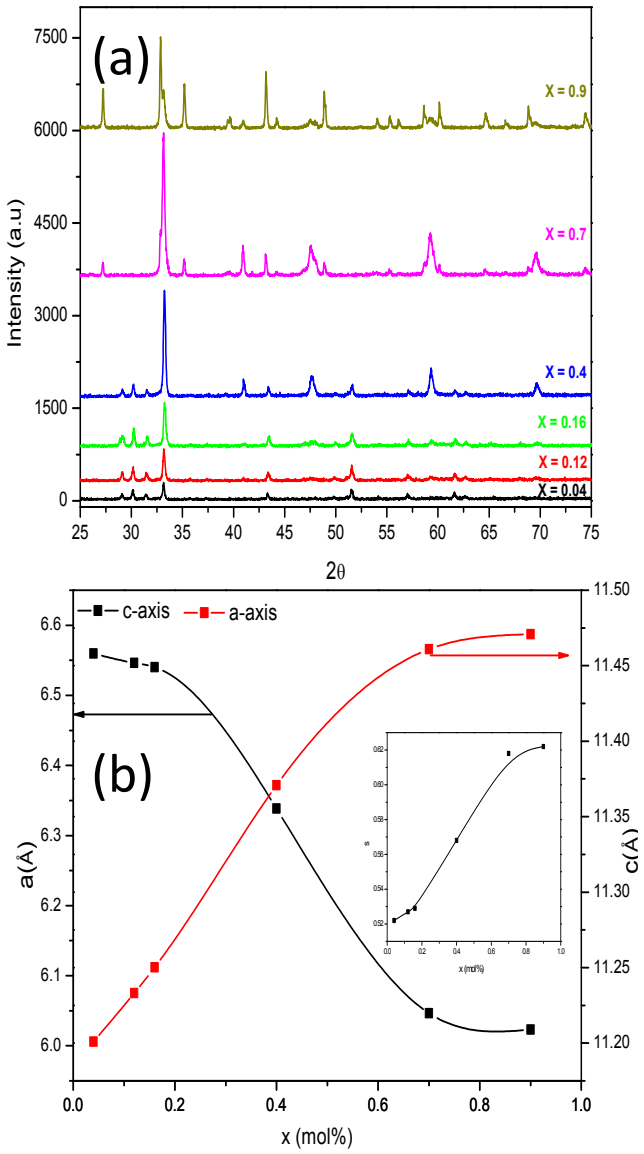

Fig. 1. (a) XRD of the Sr doped $YMnO_3$ and (b) The evolution of lattice parameters for Sr doped $YMnO_3$ ceramics of different compositions (x = 0.04, 0.12, 0.16, 0.4, 0.7 and 0.9).

Experimental

Polycrystalline samples of $Y_{1-x}Sr_xMnO_3$ (x = 0.04, 0.12, 0.16, 0.4, 0.7 and 0.9) ceramics were prepared by the conventional mixed oxide route. Analytical-grade metal oxides and carbonate powders (Y_2O_3 (99.9%), $SrCO_3$ (99.9%) and MnO_2 (99.9%) (M/S Aldrich chemicals, USA), was used as raw materials. The constituent compounds were weighed according to the required compositions and mixed for 48h using propan-2-ol and zirconia media. Then the powder was dried at 100 ^{0}C and calcined at 1000 ^{0}C for 6 h in air. The calcined fine powder was cold pressed into cylindrical pellets of 10 mm in diameter and 1-2 mm in thickness using a hydraulic press with a pressure of 50 MPa. These pellets were sintered at 1200 ^{0}C for 8 hr. The crystal structures were examined by X-ray diffraction. This was undertaken using a Philips Analytical, X'pert-MPD, employing CuKα radiation under the conditions 50kV and 40mA. The samples were scanned at an interval of 0.02^0 /min for 2θ in the range $25° \leq 2\theta \leq 75°$. The identification of the peaks was carried out using the Topas23 refinement programme. Microstructural examination of the fractured surface of the ceramics was carried out by scanning electron microscopy (SEM) (JEOL 6300 and Philips XL30, equipped with energy dispersive spectrometers (EDS) for chemical analysis. The magnetic data were recorded with the help of vibrating sample magnetometer (VSM) (Cryogenic). The zero-field-cooled (ZFC) and field-cooled (FC) measurement were performed under magnetic field (0.1T). The M(H) curves at different fixed temperature were also recorded upto 10 T. Before each ZFC measurement, samples were warmed up to 300 K and then cooled down at 5 K without filed.

Results and discussion

Sr doped $YMnO_3$ was obtained as a black, well crystallized powder. **Fig. 1 (a)** shows XRD patterns of Sr doped $YMnO_3$ at room temperature. A significant amount of the competitive hexagonal phase of the different stoichiometry was observed. X-ray diffraction analysis (XRD), carried out at room temperature, all the studied Sr doped $YMnO_3$ ceramics are monophasic and display hexagonal crystal structure. Based on the standard reference, all the observed peaks are indexed on the basis of a hexagonal unit cell of space group P63cm (JCPDS:25-1079), suggesting that all samples are pure phases without any impurity. From the XRD graph we can say that, there is a gradual intensity increasing and narrowing of the diffraction peaks, indicative of better crystallization and the grain growth with increasing Sr ratio. The lattice parameters were determined by POWD refinement method and shown in **Fig. 1(b).** With increasing of Sr ratio, the value of a lattice parameter is expanded, while the value of **c** lattice parameter decreased. The behavior of cell parameters with x can be associated with a gradually more distorted lattice, as it is shown in Fig. 1b. Important increase of the orthorhombicity s = 2(a-c)/(a+c) is noticeable along the series (see inset **Fig. 1b**). This distortion is compatible with a cooperative Jahn–Teller effect not being clear, for which x concentration starts, though it is clear for the high x content samples.

 Copyright © 2013 VBRI press

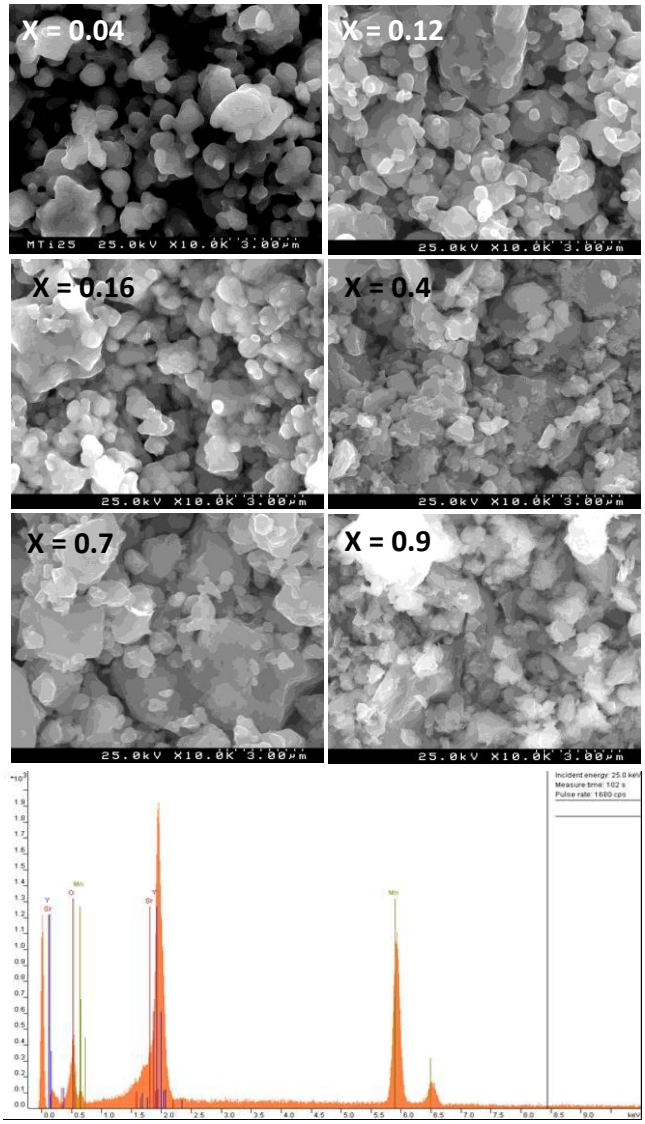

Fig. 2. SEM micrographs for Sr doped $YMnO_3$ ceramics of different compositions (x = 0.04, 0.12, 0.16, 0.4, 0.7 and 0.9) and The EDS analytic spectrum.

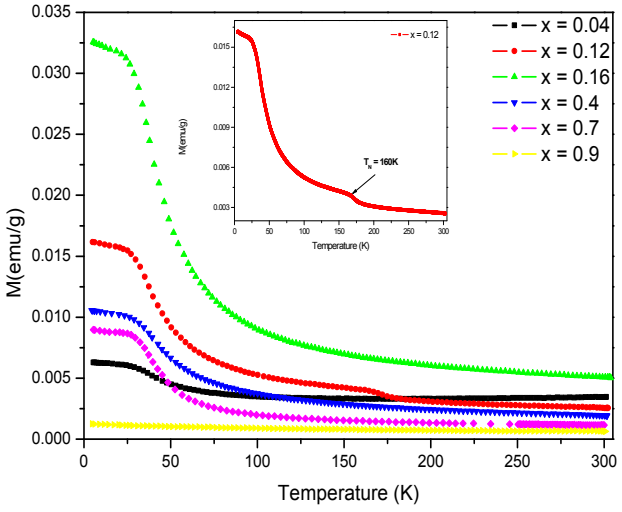

Fig. 3. Temperature dependence of magnetization for Sr doped $YMnO_3$ ceramics of different compositions (x = 0.04, 0.12, 0.16, 0.4, 0.7 and 0.9).

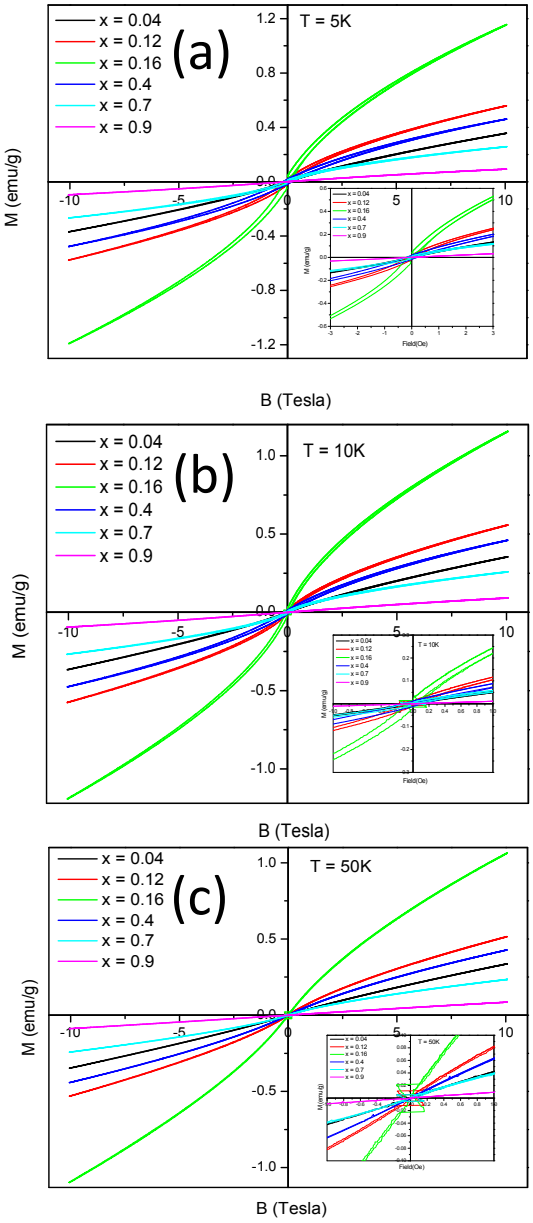

Fig. 4. (**a-c**) magnetization *versus* applied magnetic field (up to 10 Tesla) for Sr doped $YMnO_3$ ceramics of different compositions (x = 0.04, 0.12, 0.16, 0.4, 0.7 and 0.9) at T = 5K, 10K and 50K.

The microstructure, surface morphology and chemical composition of Sr doped $YMnO_3$ were studied using SEM, as shown in **Fig. 2**. Although the distribution of the grain size was inhomogeneous and decreases with the increases of concentration of Sr. The x = 0.4- 0.9 samples have dense crystalline structures and the x = 0.04-0.16 samples reveal an interconnected morphology. The grain size decreases further, suppressing the interconnected morphology. Also, the EDS analyses (**Fig. 2**) reveal that the Y/Mn ratios are very close to 1:1 for the samples studied, implying that the composition does not change during the annealing process.

The temperature-dependent magnetization curves M (T) were measured in a magnetic field of 0.1T under the conditions of field cooled (FC). **Fig. 3** displays the temperature dependence of magnetization for the samples with different composition. As can be seen, typical AFM to paramagnetic (PM) phase transition is observed for the

Copyright © 2013 VBRI press.

sample with concentration x = 0.12 and the Néel temperature (T_N) is about 160 K. With decreasing temperature, the samples with x = 0.12 exhibit a magnetic transition from a paramagnetic (PM) to a ferromagnetic (FM) state.

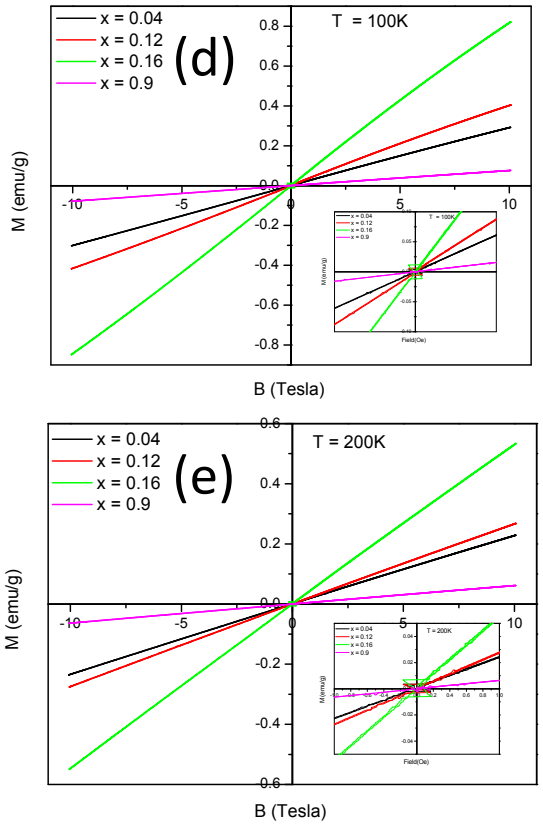

Fig. 4. (**d-e**) magnetization *versus* applied magnetic field (up to 10 Tesla) for Sr doped $YMnO_3$ ceramics of different compositions (x = 0.04, 0.12, 0.16, 0.4, 0.7 and 0.9) at T = 100K and 200K.

To further explore the magnetic properties of the samples, magnetic hysteresis loops for the Sr doped $YMnO_3$ samples with different doping have been measured at 5 K, 10K, 50K, 100K and 200K as presented in **Fig. 4 (a-e)**. For the samples with different composition, weak ferromagnetic (FM) behavior is observed with corresponding coercivity (Hc) about 300 and 200 Oe, respectively. Magnetic hysteresis curve with different composition on different temperature it shows that PM behaviour which confirms that FM component disappears above T_c. Therefore, the weak FM component does not come from FM impurity phase. As the grain size increases (with increases with Sr doping), the weak FM behavior transforms into paramagnetism. Similar effect of grain size on magnetism was also reported in nanosized YMn_2O_5 [**1**] and $BiFeO_3$ particles [**16**]. In fact, weak surface FM component is a universal feature for nanosized AFM systems, which is attributed to the deviation of the AFM arrangement to the disordered surface spin due to the lattice strain [**16, 17**]. Based on the above consideration, the magnetic structure of the nanosized $YMnO_3$ can be considered as a core/shell system, where the inner part of the particle is AFM phase and the surface is FM component. From **Fig. 5**, we observed that the maximum value of M (emu/g) is for x = 0.12 at different temperature. As we decrease the temperature the value also becomes decreases for x = 0.12. At 300 K the value of M almost same. In all samples M decreases with increases the temp except x = 0.12 and 0.16. In these compositions the value of M again increases after 200K.

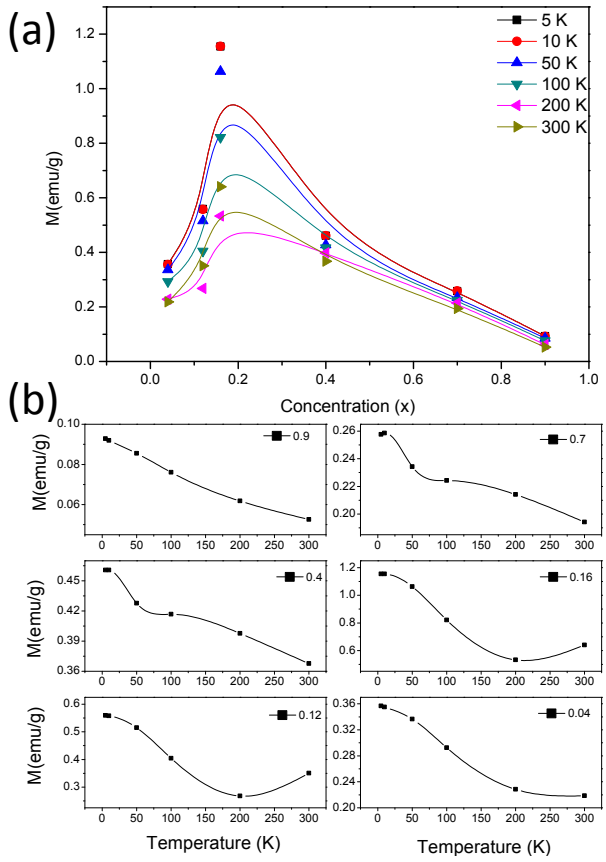

Fig. 5. (a) Maximum magnetization *versus* Concentration at different temperature and (b) Maximum magnetization *versus* temperature for Sr doped $YMnO_3$ ceramics of different compositions (x = 0.04, 0.12, 0.16, 0.4, 0.7 and 0.9).

Conclusion

We have synthesized for the first time polycrystalline samples of the orthorhombic series of $Y_{1-x}Sr_xMnO_3$ compounds with a sufficient purity that the antiferromagnetic magnetic ordering. The structural and magnetic properties of Sr doped $YMnO_3$ ceramics sintered at 1200 ^{0}C for 8 h was presented. The $Y_{1-x}Sr_xMnO_3$ (x = 0.04, 0.12, 0.16, 0.4, 0.7 and 0.9) system were successfully synthesized by high temperature solid state reaction technique. There are no structural changes observed in the samples. X-ray diffraction analysis (XRD), carried out at room temperature, all the studied Sr doped $YMnO_3$ ceramics are monophasic and display hexagonal crystal structure With increasing of Sr ratio, the value of **c** lattice parameter is expanded, while the value of **a** lattice parameter decreased. The distribution of the grain size was inhomogeneous and decreases with concentration. From magnetic mesurement we observed that for each sample both measurements (ZFC and FC) show separate M(T) curves overlapping at the highest temperature. Which was arises from the magnetic domain with different sizes. Magnetic hysteresis curve with different composition on

 Copyright © 2013 VBRI press

different temperature it shows that PM behaviour which confirms that FM component disappears above T_N. Therefore, the weak FM component does not come from FM impurity phase. As the grain size increases (with increases with Sr doping), the weak FM behavior transforms into paramagnetism.

Acknowledgements

Radheshyam Rai and Indrani Coondoo are grateful to the Foundation for Science and Technology of Portugal (FCT) for financial support (grant SFRH/BPD/38001/2007) and (grant SFRH/BPD/81032/2011) under a research project scheme.

Reference

1. Van Aken, B. B.; Palstra, T.T.M.; Filippetti, A.; Spaldin, N. A. *Nat. Mater.* 2004, 3, 164. **DOI**: 10.1038/nmat1080
2. Fiebig, M.; Lottermoser, T.; Frohlich, D.; Goltsev, A. V.; Pisarev, R. V. *Nature London* 2002, 419, 818. **DOI**: 10.1038/nature01077
3. Dho, J.; Blamire, M. G. *Appl. Phy. Lett*. 2005, 87, 252504. **DOI**: 10.1063/1.2147717
4. Kimura, T.; Goto, T.; Shintani, H.; Ishizaka, K.; Arima, T.; Tokura, Y. *Nature (London) 2003*, 426, 55. **DOI**: 10.1038/nature02018
5. Goto, T.; Kimura, T.; Lawes, G.; Ramirez, A.P.; Tokura, Y. *Phys. Rev. Lett.* 2004, 92, 257201. **DOI**: 10.1103/PhysRevLett.92.257201
6. Kenzelmann, M.; Harris, A.B.; Jonas, S.; Broholm, C.; Schefer, J.; Kim, S.B.; Zhang, C.L.; Cheong, S.W.; Vajk, O.P.; Lynn, J.W. *Phys. Rev. Lett*. 2005, 95, 087206. **DOI**: 10.1103/PhysRevLett.95.087206
7. Kimura, T.; Lawes, G.; Goto, T.; Tokura, Y.; Ramirez, A.P. *Phys. Rev. B* 2005, 71,s 224425. **DOI**:10.1103/PhysRevB.71.224425
8. Arima, T.; Tokunaga, A.; Goto, T.; Kimura, H.; Noda, Y.; Tokura, Y. *Phys. Rev. Lett.* 2006, 96, 097202. **DOI**: 10.1103/PhysRevLett.96.097202
9. Lorenz, B.; Wang, Y.Q.; Chu, C.W. *Phys. Rev. B* 2007, 76, 104405. **DOI**: 10.1103/PhysRevB.76.104405
10. Hur, N.; Park, S.; Sharma, P.A.; Ahn, J.S.; Guha, S.; Cheong, S.W. *Nature (London)* 2004, 429,392. **DOI**: 10.1038/nature02572
11. Chapon, L.C.; Blake, G.R.; Gutmann, M.J.; Park, S.; Hur, N.; Radaelli, P.; Cheong, S.W. *Phys. Rev. Lett.* 2004, 93, 177402. **DOI**: 10.1103/PhysRevLett.93.177402
12. Cruz, C.R.D.; Lorenz, B.; Sun, Y.Y.; Wang, Y.; Park, S.; Cheong, S.W.; Gospodinov, M.M.; Chu, C.W. *Phys. Rev. B* 2007, 76, 174106. **DOI**: 10.1103/PhysRevB.76.174106
13. Dong, S.; Yu, R.; Yunoki, S.; Liu, J.M.; Dagotto, E. *Eur. Phys. J. B* 2009, 71, 339. **DOI**: 10.1140/epjb/e2009-00225-1
14. Fiebig, M.; Lottermoser, T.; Frohlich, D.; Goltsev, A. V.; Pisarev, R.V. Nature London 2002, 419, 818. **DOI**: 10.1038/nature01077
15. VanAken, B. B.; Meetsma, A.; Palstra, T. T. M. *Acta Crystallogr., Sect. C: Cryst. Struct. Commun. 2001*, 57, 230. **DOI**: 10.1107/S0108270100015663
16. Muñoz, A.; Alonso, J.A.; Martínez-Lope, M.J.; Casáis, M.T.; Martínez, J.L.; Fernández-Díaz, M.T. *Phys. Rev. B* 2000, 62, 9498. **DOI**: 10.1103/PhysRevB.62.9498
17. Fiebig, M.; Frölich, D.; Kohn, K.; Leute, S.; Lottermoser, Th.; Pavlov, V.V.; Pisarev, R.V. *Phys. Rev. Lett. 2000*, 84, 5620. **DOI**: 10.1103/PhysRevLett.84.5620
18. Han, T.C.; Hsu, W.L.; Lee, W.D. *Nanoscale Research Letters*, 2011, 6, 201. **DOI**: 10.1186/1556-276X-6-201
19. Zhnag, M.F.; Liu, J.M.; Liu, Z.G. *Applied Phys. A*, 2004, 79,1753. **DOI**: 10.1007/s00339-004-2901-x
20. Zheng, H.W.; Liu, Y.F.; Zhang, W.Y.; Liu, S.J.; Zhang, H.R.; Wang, K.F. *J. Appl. Phys.* 2010, 107, 053901. **DOI**: 10.1063/1.3296323
21. Rao. G.H.; Sun, J.R.; B¨arner, K.; Hamad, N. *J. Phys.: Condens. Matter* 1999, 11, 1523. **DOI**: 10.1088/0953-8984/11/6/016
22. Zener, C. *Phys. Rev. 1951*, 82, 403. **DOI**: 10.1103/PhysRev.82.403
23. Anderson, P.W.; Hasegawa, H. *Phys. Rev.* 1955, 100, 675. **DOI**: 10.1103/PhysRev.100.675
24. De Gennes, P.G. *Phys. Rev. 1960*, 118, 141. **DOI**: 10.1103/PhysRev.118.141
25. Millis, A.J.; Littlewood, P.B.; Shraiman, B.I. *Phys. Rev. Lett. 1995*, 74, 5144. **DOI**: 10.1103/PhysRevLett.74.5144
26. Millis, A.J.; *Phys. Rev. B* 1996, 53, 8434. **DOI**: 10.1103/PhysRevB.53.8434
27. Millis, A.J.; Shraiman, B.I.; Mueller, R. *Phys. Rev. Lett.* 1996, 77,175. **DOI**: 10.1103/PhysRevLett.77.175
28. Hwang, H.Y.; Cheong, S.W.; Radaelli, P.G.; Marezio, M.; Batlogg, B. Phys. Rev. Lett. 1995, 75, 914. **DOI**: 10.1103/PhysRevLett.75.914
29. De Teresa, J.M.; Ibarra, M.R.; Garcia, J.; Blasco, J.; Ritter, C.; Algarabel, P.A.; Marquina, C.; del Moral, A. *Phys. Rev. Lett.* 1996, 76, 3392. **DOI**: 10.1103/PhysRevLett.76.3392
30. Archibald, W.; Zhou, J.S.; Goodenough, J.B. *Phys. Rev. B* 1996, 53, 14445. **DOI**: 10.1103/PhysRevB.53.14445
31. Intelligent Nanomaterials, Wiley-Scrivener Publishing LLC, USA, ISBN 978-04-709387-99, 2012.
32. Singh, M.; Kumar, M.; Štěpánek, Ulbrich, F.P.; Svoboda, P.; Santava, E.; Singla, M.L. *Adv. Mat. Lett.* 2011, 2, 409-414. **DOI**: 10.5185/amlett.2011.4257
33. Sharma, P.K.; Dutta, R.K.; Pandey, A.C. *Adv. Mat. Lett.* 2011, 2, 246-263. **DOI**: 10.5185/amlett.2011.indias214
34. Zhao, H.; Zhang, Z.; Zhao, Z.; Yu, R.; Wan, Y.; Lan, M. *Adv. Mat. Lett.* 2011, 2, 172-175. **DOI**: 10.5185/amlett.2011.1210

Advanced Materials Letters

Publish your article in this journal

ADVANCED MATERIALS Letters is an international journal published quarterly. The journal is intended to provide top-quality peer-reviewed research papers in the fascinating field of materials science particularly in the area of structure, synthesis and processing, characterization, advanced-state properties, and applications of materials. All articles are indexed on various databases including DOAJ and are available for download for free. The manuscript management system is completely electronic and has fast and fair peer-review process. The journal includes review articles, research articles, notes, letter to editor and short communications.

JOURNAL VBRI Press a rapid publication platform

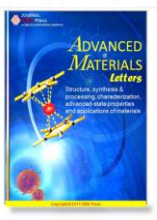

Copyright © 2013 VBRI press.